Experimental Results of the Commissioning Bundle Test QUENCH-L0 Performed in the Framework of the QUENCH-LOCA Program

J. Stuckert, M. Große, C. Rössger, M. Steinbrück, M. Walter
Karlsruhe Institute of Technology (KIT)
Hermann-von-Helmholtz-Platz 1, 76344 Eggenstein-Leopoldshafen
Tel: ++49 721 608 22558, Fax: ++49 721 608 22095, Email: juri.stuckert@kit.edu

Abstract – *The QUENCH-L0 experiment was defined as commissioning test for the new QUENCH-LOCA test series. The overall objective of this bundle test series is the investigation of ballooning, burst and secondary hydrogen uptake of the cladding under representative design basis accident conditions as well as detailed post-test investigation of cladding mechanical properties to check the embrittlement criteria. The QUENCH-L0 test bundle contained 21 electrically heated rod simulators with Zircaloy-4 claddings. Each rod was separately pressurized with krypton gas with initial pressures of 35, 40, 45, 50, and 55 bar for different rods. The transient phase with heating from 793 K to 1343 K lasted 185 s. The increased ductility of the heated cladding resulted in a progressive ballooning and consequent burst of all of the pressurized rods during the transient. The test was terminated by water quenching of the bundle without usual intermediate slow cooling phase. Post-test investigations showed strain values between 20 and 35% at cladding positions with oxidation degree corresponding to 2% ECR. Neutron radiography of cladding tubes revealed elevated concentration of absorbed hydrogen in cladding regions near to burst positions. During the tension test the cladding tubes were ruptured mostly at the middle position of burst.*

I. INTRODUCTION

Under the licensing procedures for pressurized water reactors (PWR), evidence must be produced that the impacts of all pipe ruptures hypothetically occurring in the primary loop and implying a loss of coolant can be controlled. The double-ended break of the main coolant line between the main coolant pump and the reactor pressure vessel is considered to constitute the design basis for the emergency core cooling system (ECCS) in a loss-of-coolant accident (LOCA). For the successful long-term cooling of the core a reliable sustainment of the reactor core rod geometry is required. To retain the core rod geometry it should be established the acceptable limit of cladding embrittlement, which is increased during oxidation in steam. The current LOCA criteria and their safety goals are applied worldwide with minor modifications since the NRC release in 1973 [1]. The criteria are given as limits on peak cladding temperature ($T_{PCT} \leq 1200°C$) and on oxidation level ECR (equivalent cladding reacted) calculated as a percentage of cladding oxidized (ECR $\leq 17\%$ calculated using Baker-Just oxidation correlation). These two rules constitute the criterion of cladding embrittlement due to oxygen uptake and, according to the RSK (the German Reactor Safety Commission) Guidelines, are included in current German

LOCA criteria too [2]. The results elaborated worldwide in the 1980s and 1990s on Zircaloy-4 (Zry-4) cladding tubes behavior (oxidation, deformation and bundle coolability) under LOCA conditions constitute a detailed data base and an important input for the safety assessment of LWRs [3, 4]. It was concluded that the ECC-criteria established by licensing authorities are conservative and that the coolability of an LWR and the public safety can be maintained in a LOCA. In-pile test data (with burn-up up to 35 MWd/kgU) were consistent with the out-of-pile data and did not indicate an influence of the nuclear environment on cladding deformation.

Due to different advantages the current trend in the nuclear industry is to increase fuel burn-up. At high burn-up, fuel rods fabricated from conventional Zry-4 often exhibit significant oxidation, hydriding, and oxide spallation. Thus, many fuel vendors have proposed the use of recently developed cladding alloys, such as Duplex DX-D4, M5[®], ZIRLO™ and other. Therefore, it is important to verify the safety margins for high burn-up fuel and fuel claddings with new alloys. In recognition of this, LOCA-related behaviour of new types of cladding is being actively investigated in several countries [5, 6]. Due to long cladding hydriding period for the high fuel burn-up, post-quench ductility is strongly influenced not only by oxidation but also hydrogen uptake. The 17% ECR limit is

inadequate to ensure post-quench ductility at hydrogen concentrations higher than ≈500 wppm [7]. Due to so called secondary hydriding (during oxidation of inner cladding surface after burst), which was firstly observed in JAEA [8], the hydrogen content can reach 4000 wppm in Zircaloy cladding regions around burst [9].

To investigate the influence of these phenomena on the applicability of the embrittlement criteria for the German nuclear reactors it was decided to perform the QUENCH-LOCA bundle test series at the Karlsruhe Institute of Technology (KIT) in the QUENCH facility. Compared to single-rod experiments, bundle tests have the advantage of studying the mutual interference of rod ballooning among fuel rod simulators as well as the local coolant channel blockages in a more realistic arrangement. The first experiment was performed as commissioning test with not pre-oxidised Zry-4 cladding tubes.

II. QUENCH FACILITY

The main component of the QUENCH test facility is the test section with the test bundle (Fig. 1).
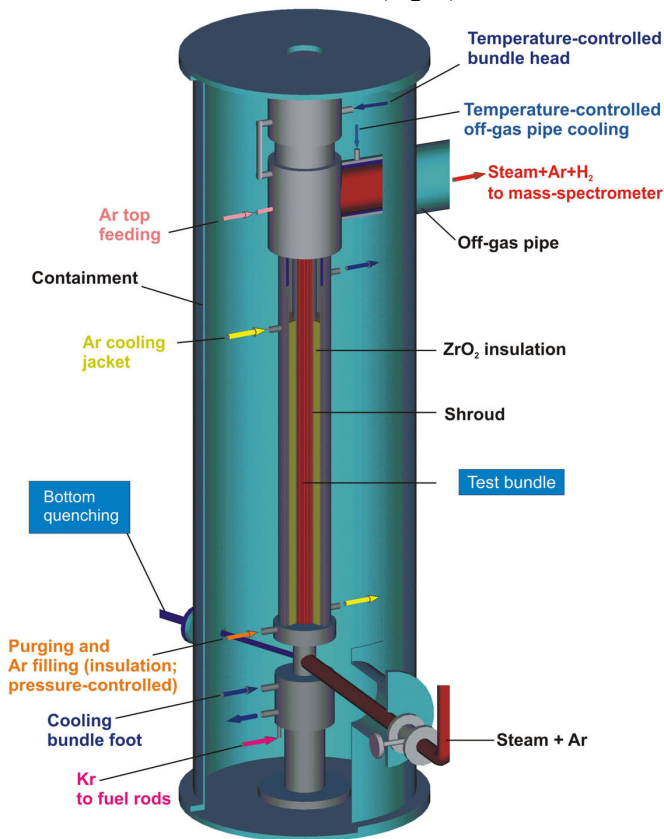
Fig. 1. QUENCH Facility: Containment and test section.

A total of 15 QUENCH high-temperature experiments on severe accident investigations were performed in this

facility between 1997 and 2009 [10]. The last two experiments within this series were conducted with M5® [11] and ZIRLO™ [12] cladding materials.

In the forced-convection mode of the QUENCH test facility, superheated steam from the steam generator and superheater together with argon as a carrier gas for off-gas measurements enter the test bundle at the bottom. The gases together with hydrogen produced in the zirconium-steam reaction flow from the bundle outlet at the top through a water-cooled off-gas pipe to the condenser where the steam is separated from the non-condensable gases. The test section has a separate inlet at the bottom to inject water for reflood (quenching).

The QUENCH-LOCA-0 test bundle is approximately 2.5 m long and is made up of 21 fuel rod simulators (Fig. 2). This "standard" bundle design is applied with a pitch of 14.3 mm. The Zry-4 cladding of the fuel rod simulator has an outside diameter of 10.75 mm and a wall thickness of 0.725 mm. The heating is electric by tungsten heaters with a diameter of 6 mm and a length of 1024 mm, installed in the rod center between bundle elevations 0 and 1024mm. The tungsten heaters are surrounded by annular ZrO_2 (yttria-stabilized) pellets, whose heat capacity of $0.9 J*K^{-1}$/pellet is comparable with the value of $1 J*K^{-1}$/pellet for UO_2 pellets. Coated electrodes of molybdenum-copper are connected to the tungsten heaters at one end and to the cable leading to the DC electrical power supply at the other end of the electrodes. Two DC-generators were used for two groups of rods connected in parallel: 1) 9 internal rods (#1 - #9) and rod #16; 2) 11 externals rods.
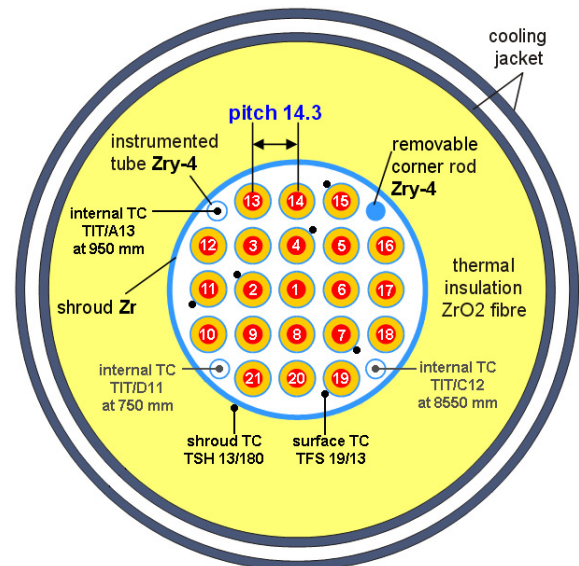
Fig. 2. Cross-section of QL0 bundle with TC at 950 mm.

The test bundle is surrounded by a Zr 702 shroud (outer diameter 86 mm), followed by a 37 mm thick ZrO_2 fiber thermal insulation axially extending from the bottom (-300 mm) to the upper end of the heated zone (+1024 mm), and a double-walled cooling jacket of Inconel 600/stainless steel over the entire length. With the shroud's inner diameter ID=80 mm the coolant channel cross section is optimized with respect to avoid a too large coolant channel area around the outer row of fuel rod simulators. Special corner rods, inserted between bundle and shroud, additionally reduce the coolant channel area to a representative value. These corner rods are either made of solid rods at the top and tubes at the bottom to be used for thermocouple instrumentation or of solid Zry-4 rods of 6 mm diameter for withdrawal from the bundle during the test to check the degree of bundle oxidation at specific times.

For temperature measurements the test bundle is equipped with NiCr/Ni thermocouples (TC) with stainless steel sheath/MgO insulation and an outside diameter of 1.0 mm. For material compatibility reasons a sleeve of zirconium is swaged onto the thermocouple sheath (Zr tube with a wall thickness of 0.35 and a length of about 20 mm). 56 surface thermocouples are resistance spot-welded to the Zry-4 cladding of the fuel rod simulators #2, 4, 7, 11, 15, 19 and distributed at 17 bundle elevations between -250 mm to 1350 mm. 16 other thermocouples have no contact with steam: 3 TCs are installed inside the corner rods and 13 TCs are located at the outer shroud surface.
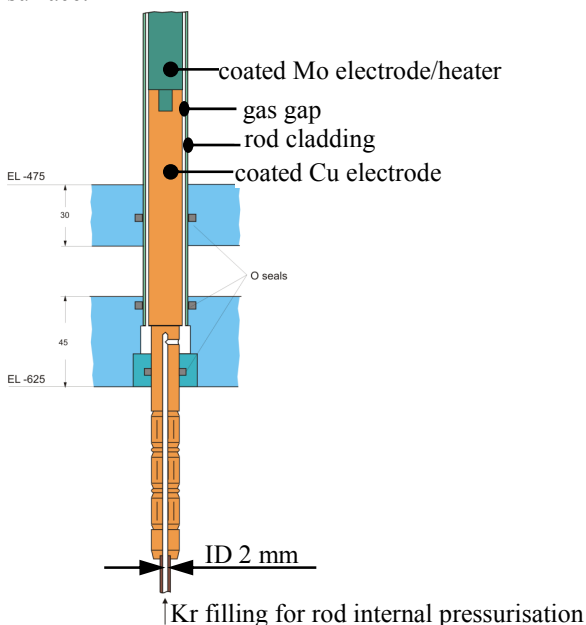
Fig. 3. Rod pressurization.

The gas supply system for individual pressurization of rods consists of pressure controller, 21 valves, 21 pressure transducers, and 21 justified compensation volumes for setting of original volume value of 31.5 cm³ (the compensation is needed because absence of empty plenums inside rod simulators). The gas supply is connected with capillary tubes to each rod at its lower end with drilled copper electrode (Fig. 3). The gas gap under cladding is: 0.15 mm in the region of Cu/Mo electrodes and 0.075 mm in the region of W-heater/ZrO_2-pellets. Before gas filling the rods and gas supply system were evacuated.

At the beginning of experiment, the fuel rod simulators were backfilled with Kr gas to 20 bar. Then, before the transient, they were separately pressurized to the target pressures of 35, 40, 45, 50, and 55 bar as shown in Fig. 4. Different pressure levels were used to investigate the pressure influence on involved processes.
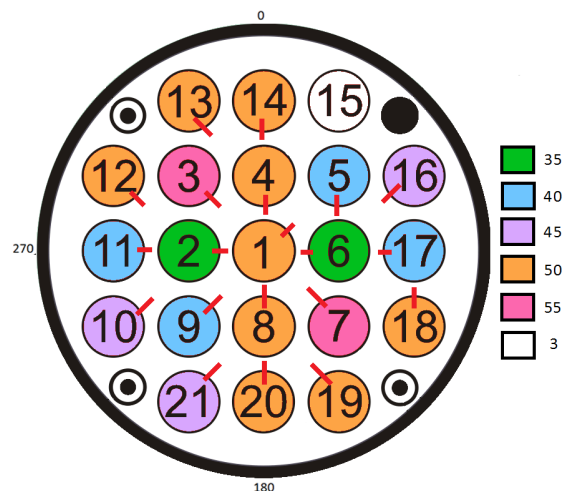
Fig. 4. Pressurization map and burst positions (red bars).

III. TEST PERFORMANCE AND PERTINENT RESULTS

The test procedure was based on pre-test calculations performed by the Paul Scherrer Institute (PSI, Villigen) using the SCDAP/RELAP5 and IBRAE (Moscow) using the SOCRAT code systems. The experiment started by stabilizing the bundle conditions with an application of electrical bundle power of 4.6 kW (corresponded the linear heat rate of ~1 W/cm) in argon - superheated steam mixture (with effective rates of 0.2 g/s/rod and 0.07 g/s/rod) resulting in maximum bundle temperatures of 800 K. The transient was initiated by rapidly increasing the electrical power to 27 kW (linear heat rate ~6 W/cm) followed by steady increase to 44 kW (linear heat rate ~10 W/cm) within 185 s. During this period the temperatures increased from their initial values to a maximum in excess of 1300 K, as planned. Fig. 5 shows the development of maximum temperature at each elevation (marking TFS x/y means a surface thermocouple for rod x at elevation y). The experiment continued with

power decrease to 3.4 kW to simulate decay heat and subsequent (after delay of 30 s) injection of steam at a nominal of 50 g/s at 215 s, resulting in immediate and rapid cooling to about 400 K which was caused by entrainment of water condensed in steam pipe line. The cooling phase was followed by a second, minor reheating to about 660 K and terminated by 90 g/s water injection at 360 s.
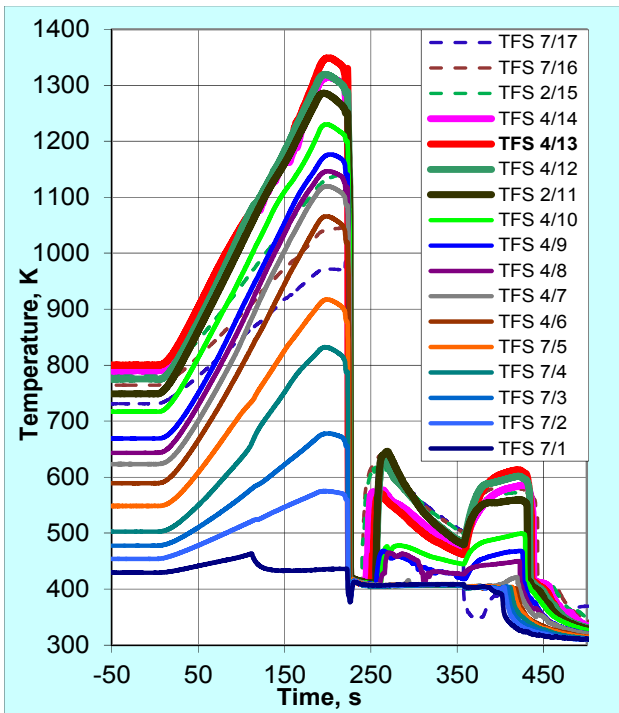
Fig. 5. Rod surface TC readings.
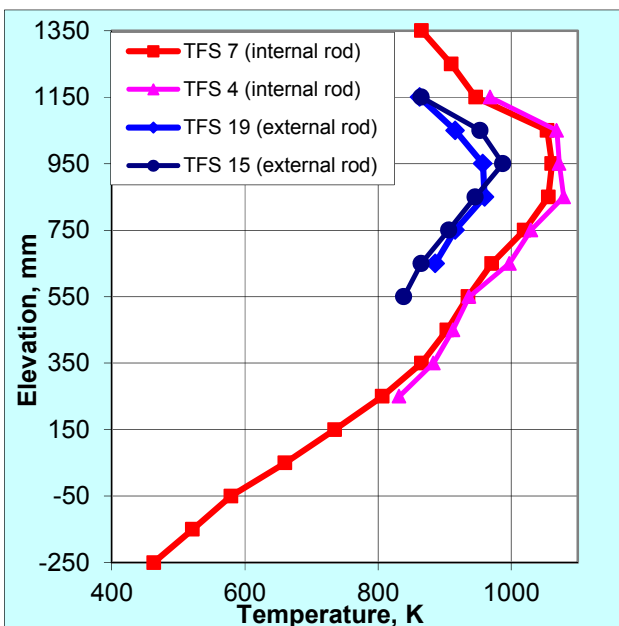
Fig. 6. Axial and radial temperature distribution at 111 s.

The axial temperature profile in the bundle has a pronounced maximum between 850 and 1050 mm (Fig. 6). There is also a radial temperature gradient due to two reasons: 1) radial heat flux to the shroud, 2) electrical power supplied to internal rod group was higher than the power for external group because both DC generators reached current limit (~3600 A) but electrical resistance of 11 external parallel connected rods is lower than for 10 internal rods.

The increased ductility of claddings during the transient phase resulted in a progressive ballooning and consequent burst of all of the pressurized rods. The first burst occurred 111 s after initiation of transient at about 1069 K at rod 1 which was pre-pressurized to 50 bar. All 20 pressurized rods failed within 63 s. (Fig. 7). The first failed rod was the central rod 1, the last one was the peripherical rod 10. The temperature range for bursts is estimated from thermocouple readings to be between 1049 and 1141 K. The burst time is mainly controlled by the rod temperature, which has a much stronger influence on the burst time than the internal pressure. The individual rod failures were indicated by internal pressure readings and precisely correlated with krypton peaks measured in the off-gas pipe by mass spectrometer.
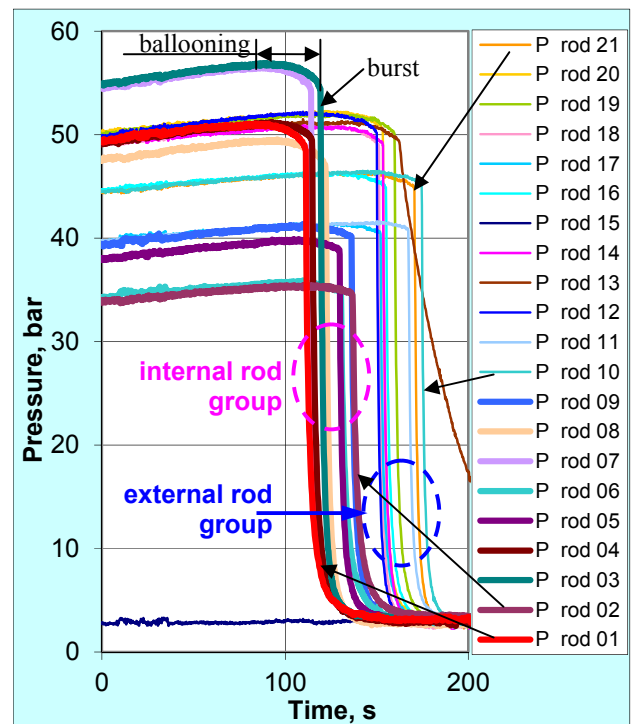
Fig. 7. Internal rod pressures during heating phase.

The radial burst positions of all rods, except the central one, correspond to the hottest rod region and are directed to the bundle center (Fig. 4). All bursts are axially

located between 930 and 1010 mm. The measured burst lengths are between 8 and 20 mm and there is no identifiable dependence on loading internal pressure. No global blockage was formed due to the scattering of the ballooning positions (Fig. 8).

All pressurized rods revealed axial contraction by ~10 mm due to Zircaloy anisotropy. No significant rod bending was observed.

Fig. 8. Bundle side view (270°) at burst region.

IV. RESULTS OF LASER PROFILOMETRY

A special laser scanner for the cladding tube profilometry was constructed by the ANT Company and installed at KIT (Fig. 9).
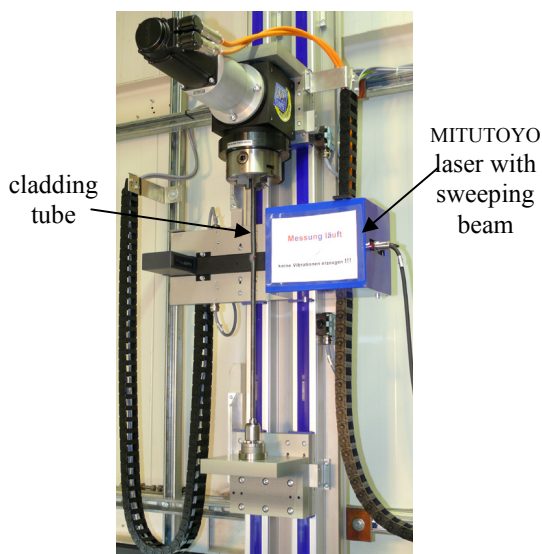
Fig. 9. ANT laser scanner

The axial and azimutal diameter changes were measured for each pressurized rod for the whole rod length with steps of 1 mm and 1° respectively. Fig. 10 shows the azimuthal rod diameter change for rod #1. For the 3D imaging of the burst region the change of rod radius was measured in cylindrical coordinates near to burst positions with the same steps width. On the basis of diameter measurements it was established that the ductile deformation of each rod extends between elevations 250 and 1250 mm (Fig. 11). The widest circumferential strain in the burst region was observed for the central rod (rod #1), i.e. for the rod which was exposed to the maximal temperature with its uniform azimuthal distribution.
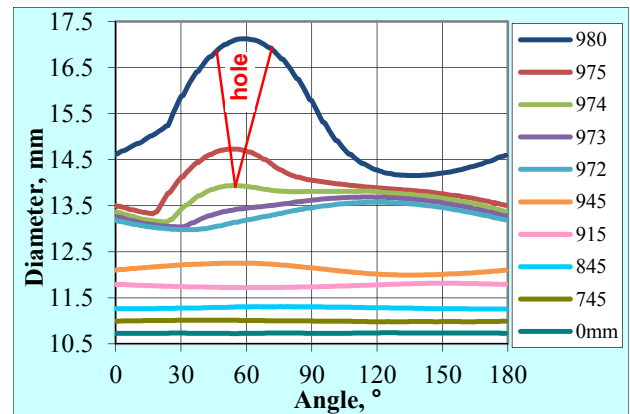
Fig. 10. Azimuthal diameter change for different elevations.
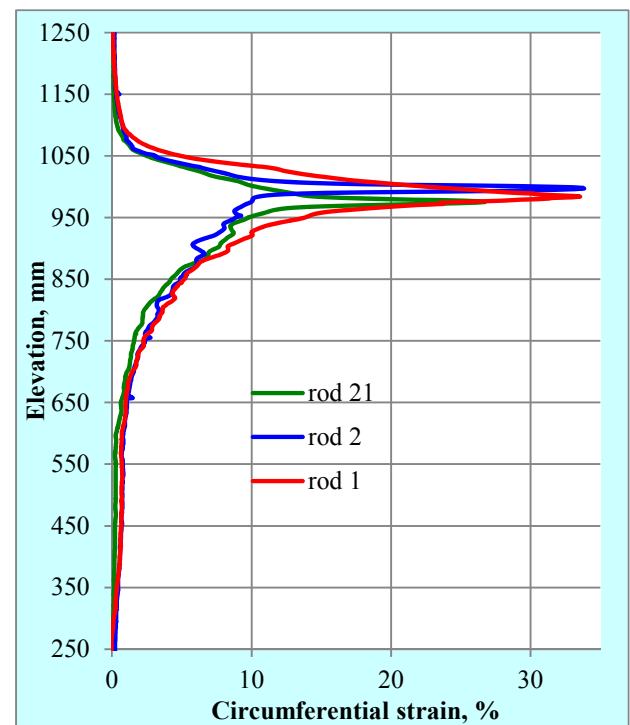
Fig. 11. Axial changing of ductile rod deformation.

Extensive data from the laser scanner measurements allows to define the degree of the bundle blockage for each elevation (Fig. 12). The blockage at all elevations is insignificant due to the relatively wide axial scattering of the maximum ballooning positions on one hand, and practical absence of touching rods on the other hand.
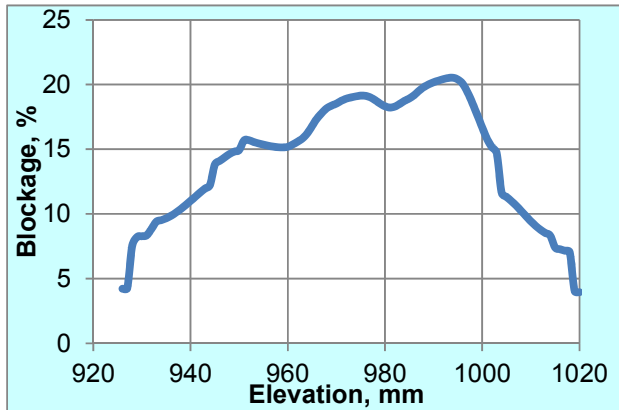
Fig. 12. Degree of cooling channel blockage.

V. NEUTRON RADIOGRAPHY INVESTIGATION OF HYDROGEN ABSOBED IN CLADDINGS

Neutron radiography is a powerful tool for the determination of hydrogen concentration and distribution in zirconium alloys [13, 14]. Hydrogen can be quantitatively and non-destructively determined with a spatial resolution of about 25 μm. The neutron radiography measurements were performed in two beam times at the ICON facility at the Swiss neutron source SINQ at Paul Scherrer Institute Villigen. Firstly, the calibration of the correlation between hydrogen concentration and total macroscopic neutron cross section was performed for the experimental setup applied. Calibration specimens were produced by annealing of Zry-4 cladding tube segments in argon/hydrogen atmosphere with different hydrogen partial pressures at various temperatures. The hydrogen uptakes of these samples were determined by measurement of the weight gain.

For the radiography investigations exposure times of 300 s per picture were applied. The investigations comprise measurements of the rods #3, #6, #8, #10, #15 and #17. The radiography of the non-pressurized rod #15 revealed that the effect of the oxide layer is not meaningful. Fig. 13 shows radiographs of the rods #3, #6 and #17. Different burst sizes are obvious. On both sides of the burst positions sloping and bended hydrogen containing darker bands can clearly be seen. Hydrogen containing bands are found in rods #3, #6 and #8 (not shown in Fig. 13) but not in the rods #10 (not shown in Fig. 13) and #17. No clear dependence of the hydrogen uptake on the inner pressure is observed. The main

parameter determining the hydrogen uptake is the time between bursting and quenching τ_Q. During this time the fill gas flows out of the burst crack. When this process is finished, the steam penetrates into the rod and oxidation of the inner cladding surface takes place in a significant manner. A threshold time seems to exists during which the fill gas flows out. This threshold is between 71 s (rod #17, no hydrogen containing band) and 93 s (rod #6, hydrogen containing band exists).
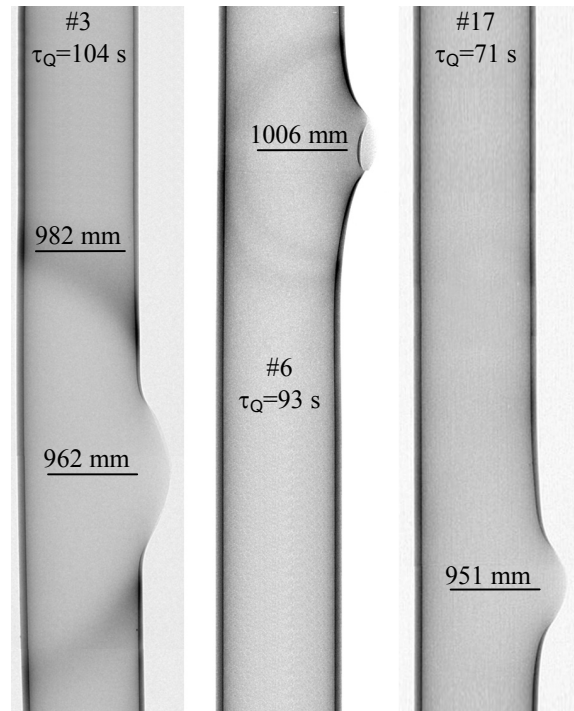
Fig. 13. Hydrogen bands around burst location.

Because of the uncertainties concerning the wall thickness and the contribution of front and rear walls to the attenuation of the neutron beam, it is not possible to determine the hydrogen concentration from radiography intensity distribution quantitatively. In order to reconstruct the specimen three-dimensionally, radiography projections have to be taken from different orientations. For the tomography, 625 projections per sample position were measured with an exposure time of 85 s per frame. Three specimens were measured, rods #1 and #3 completely and rod #5 at one side of the burst crack.

Fig. 14 shows cross sections of the reconstructed rod #1 a) in the region of a hydrogenated band and b) in the range of the burst crack. The dark region in the upper right quarter of the cladding in Fig. 14a corresponds to higher hydrogen content. The hydrogen concentration seems to be homogeneous over the cladding tube wall thickness. No regions with increased hydrogen content are in the cladding cross section at elevation of the burst center (Fig. 14b).
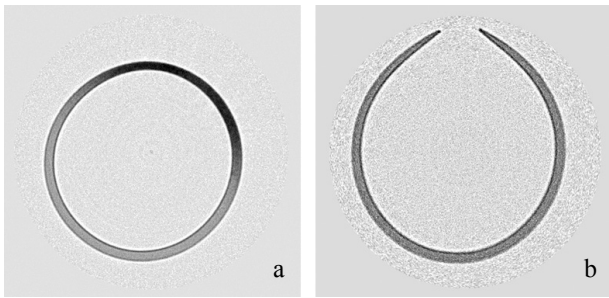
Fig. 14. Clad neutron tomography of rod #1 at 2 elevations.

Fig. 15 gives a 3D projection of the results. The blue-colored hydrogen containing bands are clearly visible. The hydrogen distribution is very complicated. The analysis is not yet finished. Maximal hydrogen concentrations of 1330, 1300 and 1060 wppm were determined for the rods #1, #3 and #5, respectively.
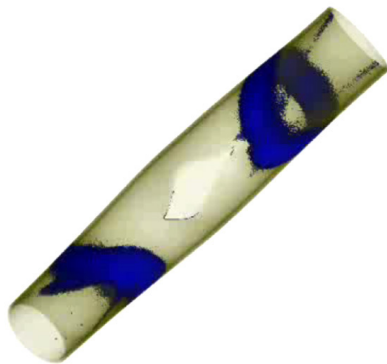
Fig. 15. Hydrogen bands inside cladding of rod #1.

VI. METALLOGRAPHIC EXAMINATION

It can be assumed that hydrogen bands are related to the boundary of the oxide layer at inner cladding surface around the burst crack. Rod #3, showing pronounced hydrogen bands, was cut into axial segments near the burst position to investigate the cladding structure. The cross section at elevation of 982 mm, which corresponds to the highest level of increased hydrogen content (Fig. 13), was investigated in detail using a Keyence digital microscope. No inner oxide layer (Fig. 16) was observed at azimuthal position of 135° corresponding to burst axial line (Fig. 4). This observation position lies above hydrogen band. The opposite cladding part at 315° is oxidized at outer as well as at inner surface (Fig. 17). This observation point is located at the beginning of hydrogen band at this azimuthal position. I. e. it could be supposed that the hydrogen band corresponds to the boundary of the inner oxidized cladding area (obviously it is the light area around burst position of rod #3 in Fig. 13).

$ZrO_2 \sim 15~\mu m$
α-$Zr(O) \sim 20~\mu m$

outer oxidized surface

inner not oxidized surface
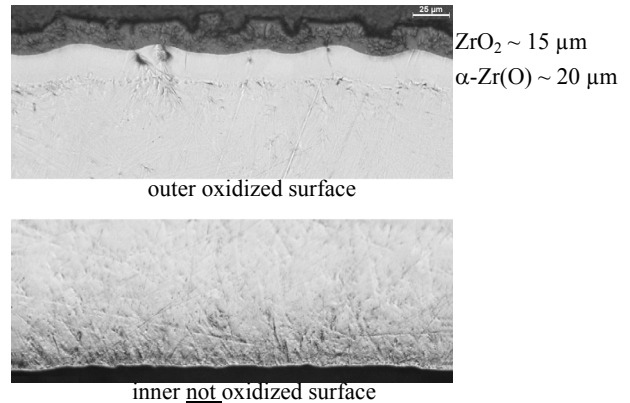
Fig. 16. Outer and inner surfaces of clad #3 at 982mm, 135°.

$ZrO_2 \sim 5~\mu m$
α-$Zr(O) \sim 11~\mu m$

outer oxidized surface

α-$Zr(O) \sim 10~\mu m$
$ZrO_2 \sim 3~\mu m$

inner oxidized surface
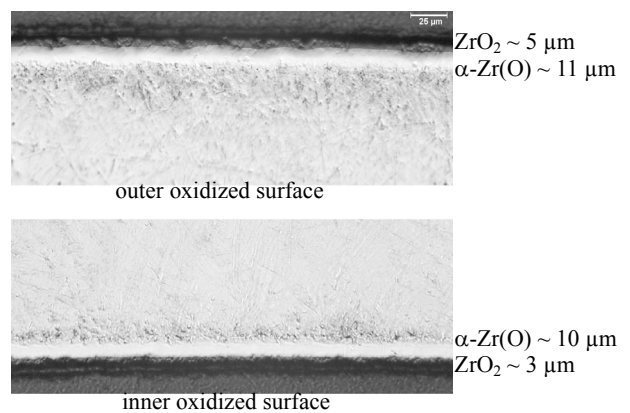
Fig. 17. Outer and inner surfaces of clad #3 at 982mm, 315°.

The outer oxide layer at azimuth of 135° (Fig. 16) is thicker than the outer oxide layer at azimuth of 315° because of higher temperature at the 135° position (this region is near to the central rod). On the other hand the oxide and α-$Zr(O)$ layers at the 135° position have pronounced wavelike structure due to plastic dilation of the cladding surface inside of axial temperature segment with maximal temperatures. Observation of the outer cladding surface of rod #3 (~980 mm, 135°) with macroscopic objective shows a characteristic "tree bark" structure (Fig. 18).
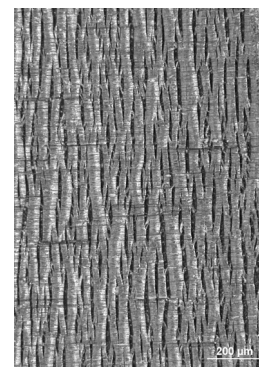
Fig. 18. Cracked structure of clad surface near to burst.

VII. RING COMPRESSION AND TENSILE TESTS

The destructive post-test examination is focused on the determination of the residual strength and ductility of tested claddings, particularly to identify the embrittlement in dependence of test conditions.

Ring-compression tests at room temperature are conducted in order to determine the embrittlement of the Zry-4 cladding as a function of the segment axial position. The results can be also used for comprehensive comparisons with results from comparable other experiments. 10-mm-long rings were compressed at a low-displacement rate (~0.03 mm/s) in an Instron testing machine (type 4505). Such kind of tests are used usually for cylindrical specimens, therefore the probes were selected at 700 and 1200 mm - far away from the burst position because the tube shape near the burst is strongly conic. Oxidation degrees at the elevation of 700 mm correspond to the ECR values of 1.3% and 0.6% for the rods #6 and #17 respectively. The corresponding load-displacement curves show typical load drops, indicating through-wall cracks along the length of the sample starting at displacements of more than 3 mm (thick curves in Fig. 19). The load-displacement curves for specimens from elevation of 1200 mm with ECR~0.3% (thin curves in Fig. 19) are practically the same as for non-oxidized (as delivered) Zircaloy tubes [15].
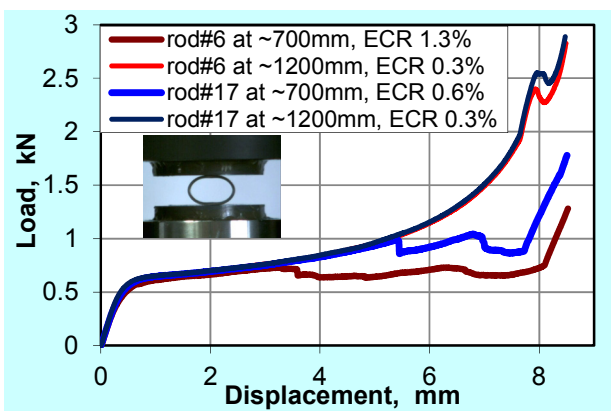
Fig. 19. Ring compression load-displacement dependence.

Since ring-compression tests do not deliver quantitative stress-strain data, additionally tensile tests were performed. These experiments were carried out on longer cladding sections (length $L_0 \sim 0.5$ m) using the same Instron testing machine, in this case equipped with special grip holders with chain link and an optical measurement system (CCD-cameras system). The optical device was used to measure the global axial deformation, as well as local axial deformations from defined (marked with white circumferential stripes) cladding sections during an experiment. Fig. 20 illustrates the dependence of tube segment elongation on degree of oxidation: the segment with less oxidation at 1140 mm shows a larger elongation in comparison to the more oxidized segment at 740 mm.
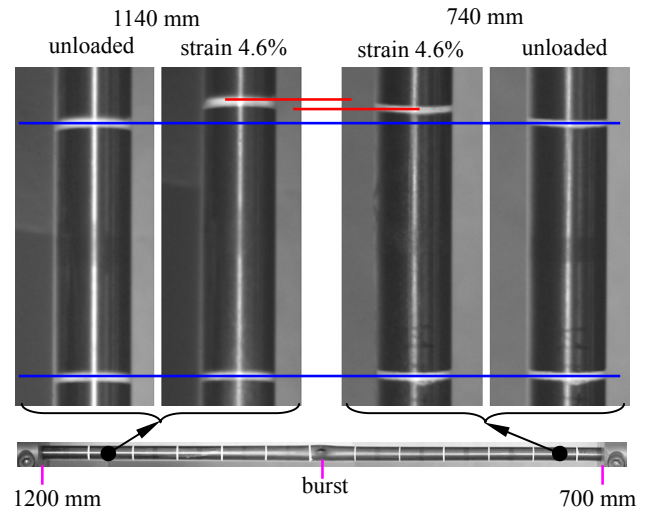
Fig. 20. Different clad elongation at two elevations.

With the global deformation, the deformation and failure behavior of the entire cladding can be determined. In Fig. 21, a diagram with selected examples of deformation curves is presented, including a picture with corresponding points of rupture.
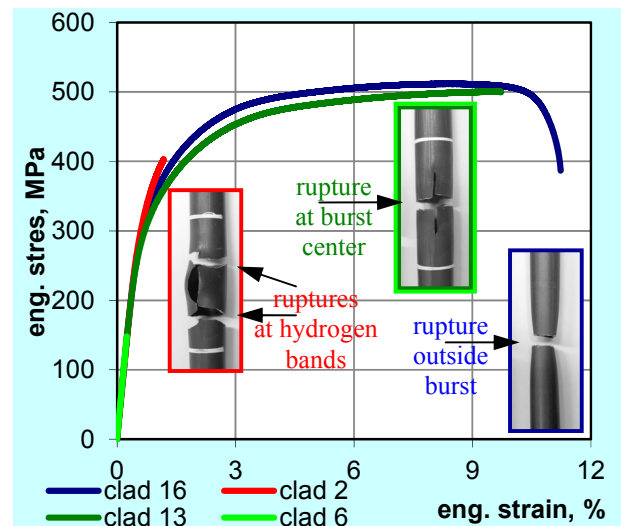
Fig. 21. Results of tensile testing for four rods.

In general it was observed, that failure is mainly influenced by the shape of the crack. If a crack edge shows a discontinuity like a buckle or a small cross crack, failure occurs independent of the tubes position in the bundle, within the burst region, based on local stress concentrations. If both crack edges exhibit a geometry free

from discontinuities, failure depends on the radial position of a cladding within the bundle. Based on a higher degree of oxidation/hydrogenation, tubes close to the bundle center fail brittle in the burst region along the hydrogen bands. Specimens from the bundle periphery show a distinctive ductile behavior and rupture occurs after necking beyond the region of considerable ballooning.

VIII. SUMMARY AND CONCLUSIONS

➢ Conduct of the QUENCH-L0 test at KIT showed qualification of the QUENCH facility for LOCA bundle tests.

➢ Data evaluation showed typical ballooning and burst processes for all 20 pressurized rods (pressure values 35, 40, 45, 50 und 55 bar). All burst cases took place during the transient heating phase at temperatures between 1053 und 1133 K. Burst opening lengths between 8 and 20 mm were measured.

➢ A recently installed laser profilometer allowed very precise und detailed measurement of cladding strain. Measured circumferential strains are between 20 und 40%. Maximal blockage of cooling channel is 21%.

➢ Investigation of outer surface of cladding upwards and downwards from burst showed development of longitudinal oxidized micro cracks, which were formed during ductile extension of metallic substrate.

➢ Oxide layers were developed on outer and inner cladding surface near to burst elevations. Only external oxide layer was observed outside away from burst positions. Maximal oxide layer thickness d_{ox}~15 μm (ECR~2%) was measured.

➢ Neutron radiography showed formation of hydrogen bands with a width of ~10 mm at the boundary of cladding inner oxidized area. Formation of this hydrogen bands was observed for rods with time interval between burst and quench initiation of more than ~90 s. The hydrogen content up to 1330 wppm at band locations was measured by means of neutron tomography.

➢ Ring compression tests showed a strong sensitivity of mechanical properties to slightly different degrees of oxidation.

➢ Two tension tests with cladding segments (length of ~500 mm) from two rods showed different rupture positions: 1) at burst center for a rod with hydrogen band (but this rupture could be intended also with prior tangential crack); 2) at a distance of about 200 mm from the burst position for the rod without hydrogen band (but the necking could be initiated by a stucked pellet). Performance of tensile testing with all 20 rods is needed to investigate the influence of hydrogen bands on the cladding failure.

REFERENCES

1. "Atomic Energy Commission Rule-Making Hearing, Opinion of the Commission", *Docket RM-50-1*, 28 December, 1973.

2. „RSK-Leitlinien für Druckwasserreaktoren". Ursprungsfassung (3. Ausgabe vom 14. Oktober 1981) mit Änderungen vom 15.11.1996. www.rskonline.de/downloads/8110dwr.pdf

3. F. J. ERBACHER and S. Leistikow. „A Review of Zircaloy Fuel Cladding Behavior in a Loss-of Coolant Accident," *Wissenschaftliche Berichte, KFK-3973*, Karlsruhe (1985).

4. G. HACHE and H. M. Chung, "The History of LOCA Embrittlement Criteria," *NUREG/CP-0172*, p. 205-237 (May 2001).

5. J.-C. BRACHET, V. Vandenberghe-Maillot, L. Portier, D. Gilbon, A. Lesbros, N. Waeckel, and J.-P. Mardon, "Hydrogen Content, Preoxidation, and Cooling Scenario Effects on Post-Quench Microstructure and Mechanical Properties of Zircaloy-4 and M5® Alloys in LOCA Conditions," *J. ASTM Intl.*, **Vol. 5**, *No. 5* (2008).

6. T. CHUTO, F. Nagase and T. Fuketa. "High Temperature Oxidation of Nb-containing Zr Alloy Cladding in LOCA Conditions," *Nuclear Engineering and Technology*, **Vol. 41**, No.2 (March 2009).

7. H. M. CHUNG. "Fuel Behavior under Loss-of-Coolant Accident Situations," *Nuclear Engineering and Technology*, **Vol. 37**, *No.4* (August 2005).

8. H. UETSUKA, T. Furuta and S. Kawasaki. "Zircaloy-4 Cladding Embrittlement due to Inner Surface Oxidation under Simulated Loss-of-Coolant Condition," *Journal of Nuclear Science and Technology*, **Vol. 18[9]**, p. 705-717 (September 1981).

9. M. BILLONE, Y. Yan, T. Burtseva, R. Daum. "Cladding Embrittlement During Postulated Loss-of-Coolant Accidents," **NUREG/CR-6967** (July 2008).

10. M. STEINBRÜCK, M. Große, L. Sepold, J. Stuckert, „Synopsis and outcome of the QUENCH experimental program," *Nuclear Engineering and Design*, **Vol. 240,** p.1714–1727 (2010).

11. J. STUCKERT, J. Birchley, M. Grosse, B. Jaeckel, M. Steinbrück. „Experimental and calculation results of the integral reflood test QUENCH-14 with M5[®] cladding tubes," *Annals of Nuclear Energy*, **Vol. 37**, p. 1036–1047 (2010).

12. J. STUCKERT, M. Große, M. Steinbrück, „Experimental Results of Reflood Bundle Test QUENCH-15 with ZIRLO™ Cladding Tubes," *Proceedings of ICAPP'10*, San Diego, June 13-17, Paper 10286 (2010).

13. M. GROSSE, G. Kuehne, M. Steinbrueck, E. Lehmann, J. Stuckert, P. Vontobel,: „Determination of the hydrogen uptake of steam-oxidised zirconium alloys by means of quantitative analysis of neutron radiographs," *Journal of Physics Condensed Matter* **Vol. 20**, *Issue 10*, Article number 104263 (March 2008).

14. M. GROßE, E. Lehmann, M. Steinbrück, G. Kühne, J. Stuckert, „Influence of oxide layer morphology on hydrogen concentration in tin and niobium containing zirconium alloys after high temperature steam oxidation," *Journal of Nuclear Materials*, **Vol. 385**, *Issue 2*, Pages 339-345 (March 2009).

15. M. WALTER. "Mechanical Tests on Claddings in the Framework of the QUENCH-LOCA Programme". *Proceedings of 15th International QUENCH Workshop*, ISBN 978-3-923704-71-2, Karlsruhe (November 2009).